Hindawi Publishing Corporation
Journal of Nanomaterials
Volume 2015, Article ID 659402, 8 pages
http://dx.doi.org/10.1155/2015/659402

Research Article

Ni/SiO_2 Catalyst Prepared with Nickel Nitrate Precursor for Combination of CO_2 Reforming and Partial Oxidation of Methane: Characterization and Deactivation Mechanism Investigation

Sufang He,[1] Lei Zhang,[2] Suyun He,[2] Liuye Mo,[3] Xiaoming Zheng,[3] Hua Wang,[1] and Yongming Luo[2]

[1]*Research Center for Analysis and Measurement, Kunming University of Science and Technology, Kunming 650093, China*
[2]*Faculty of Environmental Science and Engineering, Kunming University of Science and Technology, Kunming 650500, China*
[3]*Institute of Catalysis, Zhejiang University, Key Lab of Applied Chemistry of Zhejiang Province, Hangzhou 310028, China*

Correspondence should be addressed to Yongming Luo; environcatalysis222@yahoo.com

Received 5 August 2014; Revised 6 January 2015; Accepted 6 January 2015

Academic Editor: Mohamed Bououdina

The performance of Ni/SiO_2 catalyst in the process of combination of CO_2 reforming and partial oxidation of methane to produce syngas was studied. The Ni/SiO_2 catalysts were prepared by using incipient wetness impregnation method with nickel nitrate as a precursor and characterized by FT-IR, TG-DTA, UV-Raman, XRD, TEM, and H_2-TPR. The metal nickel particles with the average size of 37.5 nm were highly dispersed over the catalyst, while the interaction between nickel particles and SiO_2 support is relatively weak. The weak NiO-SiO_2 interaction disappeared after repeating oxidation-reduction-oxidation in the fluidized bed reactor at 700°C, which resulted in the sintering of metal nickel particles. As a result, a rapid deactivation of the Ni/SiO_2 catalysts was observed in 2.5 h reaction on stream.

1. Introduction

The Ni-based catalyst has recently attracted considerable attention due to the plentiful resources of nickel, as well as its low cost and good catalytic performance comparable to those of noble metals for many catalytic reactions, such as hydrogenation of olefins and aromatics [1], methane reforming [2], and water-gas shift reaction [3]. Therefore, Ni-based catalyst is believed to be the most appropriate catalyst applied in the industrial process [4–6]. It is generally accepted that the catalytic performance of Ni-based catalyst is closely related to several parameters, including the properties of support, preparation method, and active phase precursor employed.

Support plays an important role in determining the performance of Ni-based catalyst. Generally, a support with high surface areas is very necessary since it is effective in increasing Ni dispersion and improving thermal stability, hence not only providing more catalytically active sites, but also decreasing the deactivation over time of the catalysts due to sintering and migration effects [7, 8]. For its good thermostability, availability, and relative high specific surface area, SiO_2 support was widely used for preparing Ni-based catalyst [9]. In particular, spherical silica is successfully used as a catalyst support in fluidized bed reactor due to its high mechanical strength.

The method of catalyst preparation is another key parameter which needs to be optimized because it will result in different structural and textural properties of Ni-based catalyst. Therefore, numerous methods, including precipitation, homogeneous deposition-precipitation, and sol-gel techniques, have been developed to enhance the performance of Ni-based catalyst [10–18]. However, allthe above methodologies mentioned are too complex or expensive to scale

up in industry. The incipient wetness impregnation (IWI) is one of the most extensively used method [19–23] due to its simplicity in practical execution on both laboratory and industrial scales, in addition to its facility in controlling the loading amount of the active ingredient.

In addition, the choice of the precursor salt is also crucial since it determines whether the Ni-based catalyst will be prepared successfully or not. As an efficient precursor, two terms must be met: firstly, high solubility is desirable because the precursor concentration in the impregnation solution must be high [24]; secondly, the ability to be decomposed during calcinations is prerequisite since the precursor must be fully transformed into oxide particles without leaving side species that may modify the properties of the support [24]. As a result, owing to its commercial availability and low cost, as well as its high solubility in water and effortless decomposition at moderate temperatures, nickel nitrate is the precursor most often used in the preparation of Ni-based catalyst [23, 24].

In this paper, Ni/SiO_2 catalyst was prepared by incipient wetness impregnation (IWI) with nickel nitrate as precursor and tested in the process of combination of CO_2 reforming and partial oxidation of methane (CRPOM) to produce syngas. TG-DTA, HR-TEM, IR, UV-Raman, XRD, and H_2-TPR were employed to characterize the Ni/SiO_2 catalysts in detail to reveal the relationship between synthesis, properties, and catalytic performances as well as to investigate the causes of deactivation.

2. Experimental Section

2.1. Catalyst Preparation. The Ni/SiO_2 catalysts were prepared with IWI using nickel nitrate as precursor according to our previous works [21, 22]. The SiO_2 was commercially obtained (S_{BET} = 498.8 m^2/g, Nanjing Tianyi Inorganic Chemical Factory). Prior to use, the SiO_2 was pretreated with 5% HNO_3 aqueous solution for 48 h and then washed with deionized water until the filtrate was neutrality. The size of SiO_2 was selected between 60 and 80 mesh. It was then impregnated with an aqueous solution of nickel nitrate. The obtained sample was dried overnight at 100°C and subsequently calcined in air at 700°C for 4 h. Unless otherwise stated, the loading of Ni was 3 wt%, and the calcination temperature was 700°C. The Ni/SiO_2 catalyst was designated as 3NiSN.

2.2. Catalytic Reaction. The catalytic reaction was performed in a fluidized-bed reactor that was comprised of a quartz tube (I.D. = 20 mm, H = 750 mm) under atmospheric pressure at 700°C. Prior to reaction, 2 mL of catalyst was reduced at 700°C for 60 min under a flow of pure hydrogen at atmospheric pressure with a flow rate of 50 mL/min. A reactant gas stream that consisted of CH_4, CO_2, and O_2, with a molar ratio of 1/0.4/0.3, was used with a gas hourly space velocity (GHSV) of 9000 h^{-1}. The feed gas was controlled by mass flow controllers. The effluent gas cooled in an ice trap was analyzed with an online gas chromatograph that was equipped with a packed column (TDX-01) and a thermal conductivity detector. Under our reaction conditions, the oxygen in the feed gas was completely consumed in all cases.

2.3. Catalyst Characterization. FTIR spectra were measured using a Nicolet 560 spectrometer equipped with a MCT detector. The samples were tabletted to thin discs with KBr.

Thermogravimetric analysis (TGA) and differential thermal analysis (DTA) were performed on a PERKIN ELMER-TAC7/DX with a heating rate of 10°C/min under oxygen (99.99%, 20 mL/min). The samples were pretreated with oxygen flow at 383 K for 1 h.

UV-Raman spectra were carried out with a Jobin Yvon LabRam-HR800 instrument, using 325.0 nm Ar^+ laser radiation. The excitation laser was focused down into a round spot approximately 2 μm in diameter. The resolution was 4 cm^{-1} and 1000 scans were recorded for every spectrum. The catalysts were ground to particle diameters < 150 μm before analysis.

X-ray powder diffraction (XRD) patterns of samples were obtained with an automated power X-ray diffractometer (Rigku-D/max-2550/PC, Japan) equipped with a computer for data acquisition and analysis, using Cu Kα radiation, at 40 kV and 300 mA. The reduced samples were priorly reduced at 700°C for 1 h and cooled to room temperature in hydrogen atmosphere, but the fresh samples were used directly after calcined in air at 700°C for 4 h. All the samples were ground to fine powder in an agate mortar before XRD measurements.

Transmission electron microscopy (TEM) images were recorded on a Philips-FEI transmission electron microscope (Tecnai G2 F30 S-Twin, Netherlands), operating at 300 kV. Samples were mounted on a copper grid-supported carbon film by placing a few droplets of ultrasonically dispersed suspension of samples in ethanol on the grid, followed by drying at ambient conditions.

H_2-temperature-programmed reduction (H_2-TPR) experiments were performed in a fixed-bed reactor (I.D. = 4 mm). 50 mg samples were used and reduced under a stream of 5% H_2/N_2 (20 mL/min) from 50°C to 800°C with a ramp of 7°C/min. Hydrogen consumption of the TPR was detected by a TCD and its signal was transmitted to a personal computer.

The experiments for reduction-oxidation cycle (redox) performance were performed as follows. The catalysts were pretreated with H_2 flow at 700°C for 1 h and then were cooled down to room temperature and reoxidized in O_2 at different temperature for 1 h. The reoxidized samples were then performed by H_2-TPR experiments as above.

3. Results and Discussion

3.1. Catalytic Activity Measurements. The catalytic performance of Ni/SiO_2 was shown in Figure 1. A rapid deactivation was detected for the 3NiSN, and the corresponding conversion of CH_4 (X_{CH4}) decreased from ~58% to ~25% within 1.5 h reaction on stream. In order to investigate the causes of deactivation, the 3NiSN catalyst was characterized by TG-DTA, HR-TEM, IR, UV-Raman, XRD, and H_2-TPR in detail.

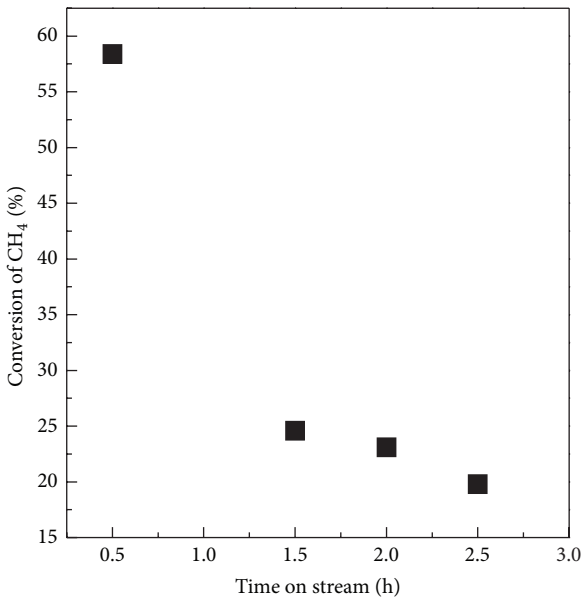

FIGURE 1: CH_4 conversion versus time on 3NiSN catalyst for combination of CO_2 reforming and partial oxidation of methane to produce syngas (reaction temperature: 700°C, $CH_4/CO_2/O_2$ = 1/0.4/0.3, and GHSV = 9000 h^{-1}).

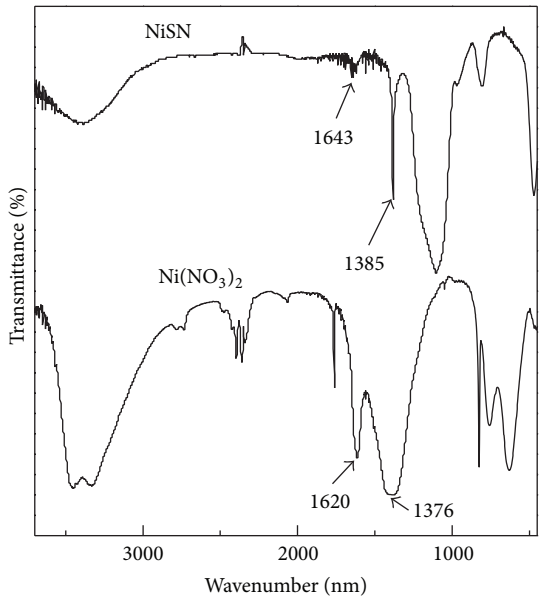

FIGURE 2: FT-IR spectra of 3NiSN (dried at 100°C) and nickel nitrate ($Ni(NO_3)_2$).

3.2. Catalyst Characterization Results

3.2.1. FT-IR Analysis. The FT-IR spectra of 3NiSN before calcination and $Ni(NO_3)_2$ precursor were illustrated in Figure 2. Two intense bands of $Ni(NO_3)_2$ centered at 1620 cm^{-1} and 1376 cm^{-1} were ascribed to asymmetric and symmetric vibrations of nitrate, respectively [25]. After $Ni(NO_3)_2$ being impregnated on SiO_2, the position of the two bands of $Ni(NO_3)_2$ shifted to higher wavenumber about 1643 cm^{-1} and 1385 cm^{-1}, respectively. Similar to our previous study [23], this shift to higher wavenumber might be contributed to the interaction between nickel nitrate and support SiO_2.

3.2.2. Thermal Analysis. In order to study the formation of NiO from precursor, thermal analysis of 3NiSN before calcination was carried out (shown in Figure 3). The extra water should be removed by holding the precursor under O_2 at 110°C for 1 h. The thermal oxidation degradation of the dried 3NiSN consisted of two main steps. The first weight loss (9.1 wt%) at 110–240°C region in TG together with a differential peak at around 224°C in DTG curve was probably due to the dehydration of 3NiSN. The second large weight loss at region of 240–380°C (11.1 wt%) in TG, accompanied with a small endothermic peak around 293°C in DTA, had been attributed to thermoxidative degradation of nickel nitrate. This decomposition step exhibited a differential peak around 277°C in DTG profile. Above 380°C, practically weight loss could not be observed any more. The TG-DTA curves confirmed the absolute volatility of water and nitrate and also the formation of NiO over catalysts around 380°C. The calcination of 3NiSN beyond 380°C would enhance the interaction between the NiO and SiO_2 support, according to our earlier study [23].

3.2.3. UV-Raman Analysis. Further evidence for the formation of NiO might be drawn from UV-Raman spectra exhibited in Figure 3. Herein, the spectrum for NiO was included as a reference. As seen from Figure 4, the intense and sharp peak at 1139 cm^{-1}, together with three weak peaks at 900, 732, and 578 cm^{-1}, was assigned to the Raman responses of NiO. Similar to NiO reference, the peaks of 3NiSN center at about 1135, 900, 726, and 580 cm^{-1} were also attributed to NiO. Furthermore, compared with the reference of NiO, the four Raman peaks of NiO over 3NiSC appeared more intensive, thus suggesting that the NiO particles over 3NiSN catalyst were larger [23, 26, 27].

3.2.4. XRD Analysis. XRD measurements were carried out to understand the crystalline structure of 3NiSN catalysts, and the results were presented in Figure 5. The XRD patterns of all samples exhibited a broad and large peak around 22°, which was attributed to amorphous silica of support. After calcination, the sample showed only the fcc-NiO phase, with typical reflections of the (111), (200), and (220) planes at 2θ = 37°, 43°, 63°, respectively. After being reduced with H_2 for 4 h, the peaks assigned to NiO disappeared, and three other peaks around 44°, 52°, and 76° for Ni (111), Ni (200), and Ni (220) planes were detected, thus inferring the successful transformation of NiO to metallic Ni after reduction with H_2.

3.2.5. TEM Analysis. Further insight on the aggregation of Ni particles over the 3NiSN could be obtained by TEM analysis. Figures 6(a) and 6(b) exhibited the TEM images of 3NiSN after reduction and deactivation, respectively. The Ni particles over both catalysts were approximately spherical in shape. Highly dispersed Ni particles were detected for the Ni/SiO_2 just after reduction. However, obvious glomeration

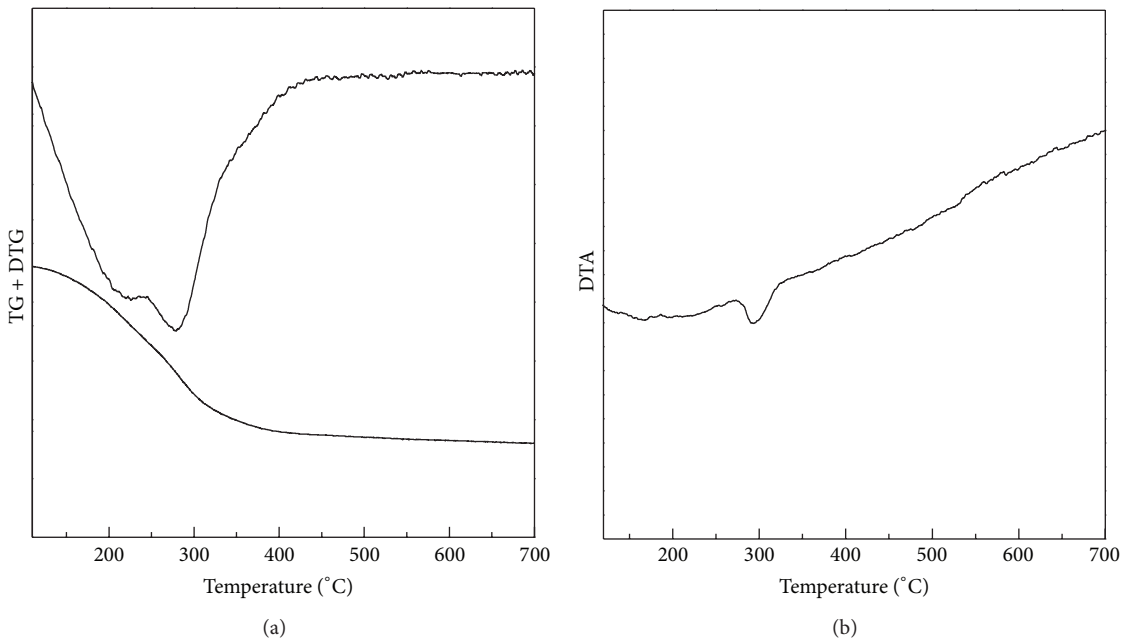

Figure 3: (a) TG + DTG and (b) DTA thermogram of 3NiSN dried at 100°C.

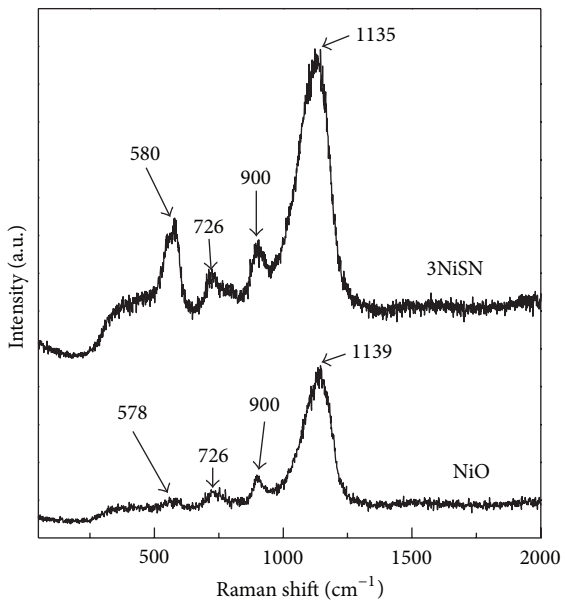

Figure 4: UV-Raman spectra of 3NiSN (calcined at 700°C for 4 h) and NiO (as a reference).

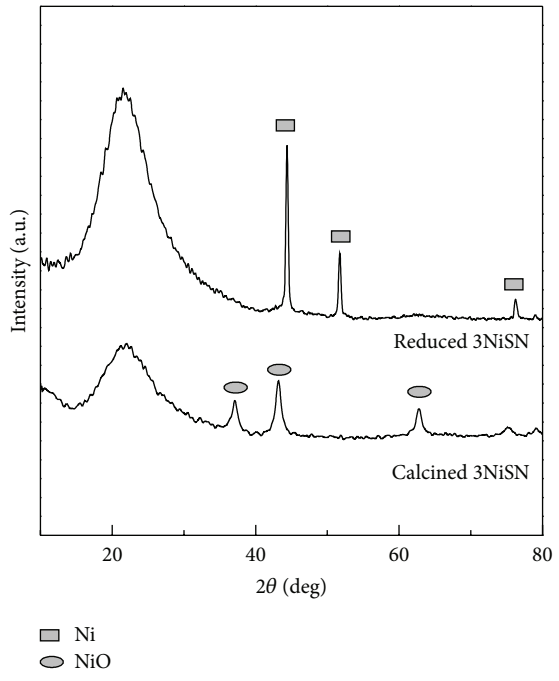

Figure 5: XRD patterns of 3NiSN before and after reduction in H_2 for 4 h.

of Ni particles was observed for the 3NiSN catalyst after deactivation. In order to make a profound analysis, the corresponding particle size distributions obtained from TEM were summarized in Figures 6(c) and 6(d) for 3NiSN after reduction and deactivation, respectively. The particle size values of reduced 3NiSN were distributed in a range of 16.1–84.0 nm with the average size around 37.5 nm. As for 3NiSN after deactivation, the mean size increased to 50.4 nm with distributed range of 36.0–73.6 nm. An evident particle aggregation was formed over 3NiSN catalyst, which was in accordance with the XRD result.

3.2.6. H_2-TPR Analysis. TPR is an efficient method to characterize the reducibility of supported nickel-based catalysts.

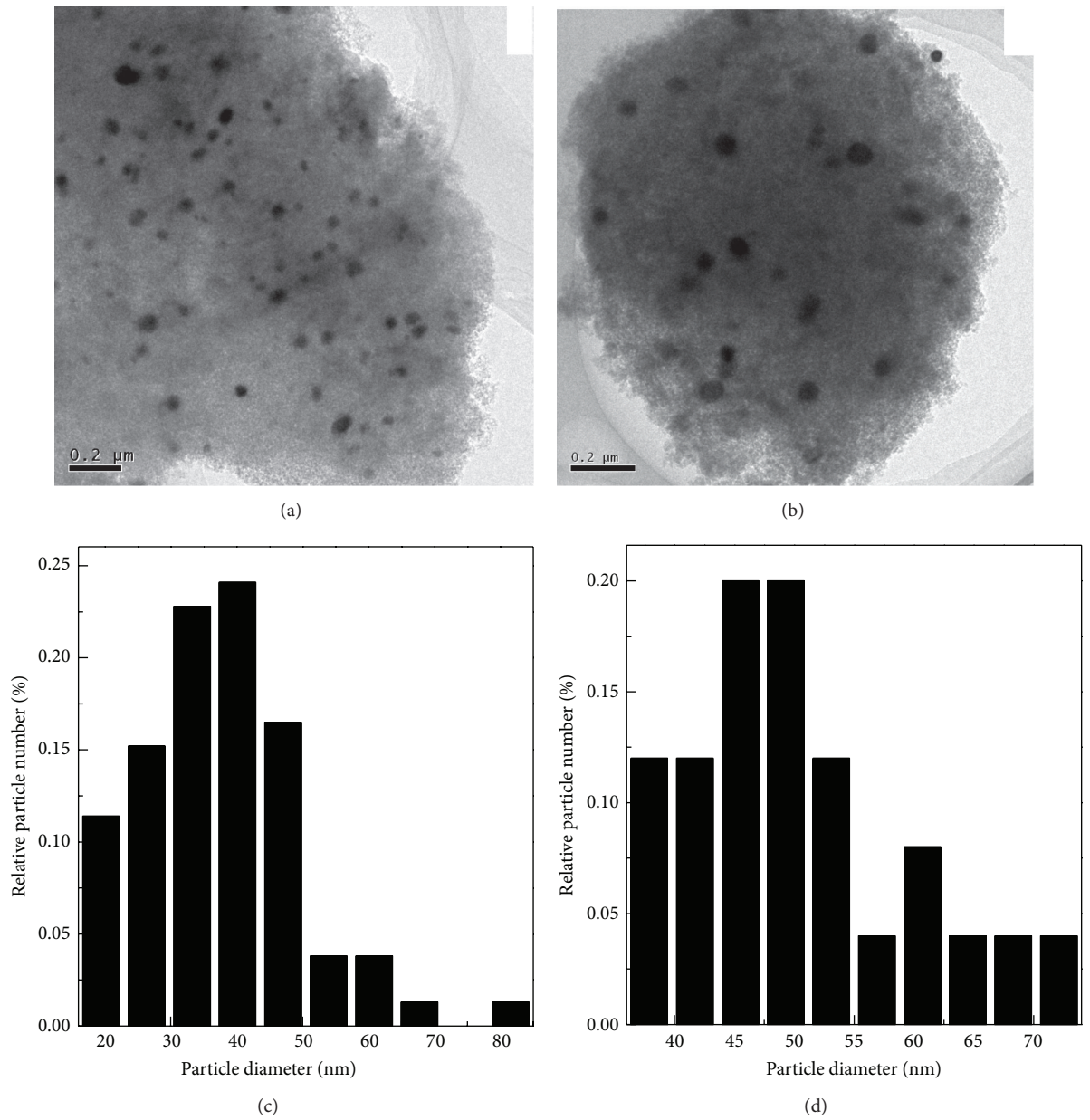

Figure 6: TEM images of (a) reduced 3NiSN and (b) deactivated 3NiSN, and histogram of the particle size distribution obtained from sampling of nanoparticles from TEM data (c) for reduced 3NiSN and (d) for deactivated 3NiSN.

TPR profiles of 3NiSN catalysts were depicted in Figure 7. Two reduction peaks were observed for the fresh 3NiSN catalyst (just calcined) at 430°C and 450°C. The low-temperature peak might be contributed to the reduction of NiO which is negligible weak interaction with SiO_2. The high-temperature peak was caused by the reduction of nickel oxide which interacted weakly with SiO_2. Furthermore, ttthe reduction-oxidation cycle (redox) performance of a catalyst would strongly influence the catalytic activity for an oxidation involved reaction [28]. Therefore, the redox performances of 3NiSN catalysts were investigated, and the corresponding experiment results were depicted in Figure 7. After being reduced in H_2 flow at 700°C for 1 h, the 3NiSN catalysts were reoxidized in O_2 at different temperatures and then tested with H_2-TPR. No clear reduction peak of NiO was detected for 3NiSN with reoxidized temperature below 300°C. As reoxidization temperature increased from 400 to 700°C, the rereduction temperature increased from ~290 to ~370°C; however, it was always less than the temperature needed to reduce the NiO of fresh 3NiSN. Distinctly, the weak NiO-SiO_2 interaction over 3NiSN catalyst disappeared with repeating oxidation-reduction-oxidation process. Studies from the previous work show that the strong interaction between NiO and support could suppress efficiently the sintering of

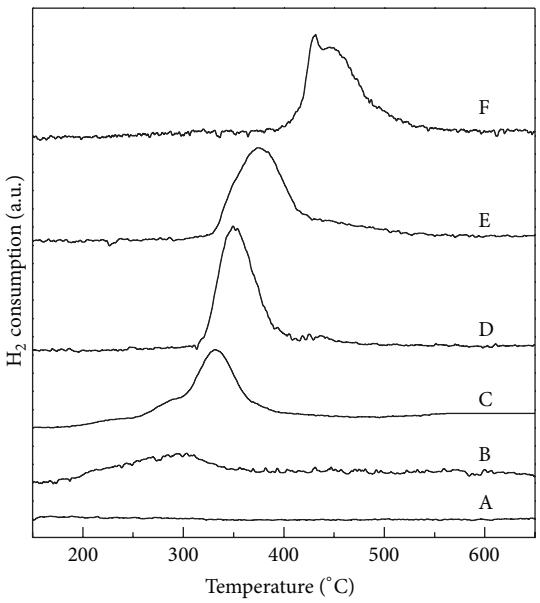

Figure 7: The reduction-oxidation cycle (redox) performance of 3NiSN catalysts with different reoxidization temperature (A: 300°C; B: 400°C; C: 500°C; D: 600°C; E: 700°C; F: fresh, just calcined).

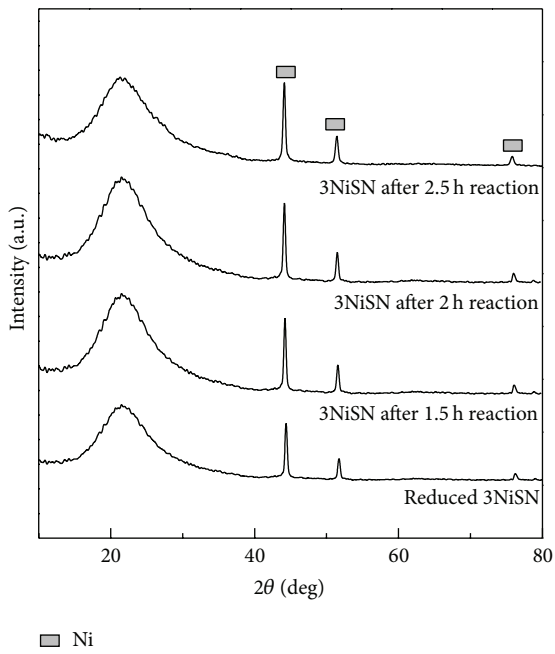

Figure 8: The effect of reaction time on the XRD patterns of 3NiSN.

metallic nickel [21–23]. Therefore, the disappearance of NiO-SiO_2 interaction would lead to the sintering of active nickel particles at high reaction temperature.

3.2.7. Effect of the Particle Size of Ni. It is generally accepted that the crystalline size of metallic nickel plays an important role in the catalytic performance for nickel-catalyzed reactions: smaller metallic Ni size helps to provide more active sites to reach the much better catalytic activity. Our previous works had also demonstrated this view [21, 22]. In order to investigate the particle size dependence of the catalytic reaction, the 3NiSN catalysts after different time (1.5 h, 2.0 h, and 2.5 h) reaction on stream were taken out to be estimated by XRD and calculated with the Scherrer equation (shown in Figure 8). For all the 3NiSN (even after deactivation), only Ni and amorphous SiO_2 phase detected by XRD. No NiO phase was found, which meant no significant change in Ni phase was observed for 3NiSN even after deactivation. Noteworthily, the diffraction intensity of nickel crystalline increased with reaction time, which indicated the crystalline size of nickel on 3NiSN increased with reaction time. The crystalline size of nickel on 3NiSN as a function of reaction time was shown in Figure 9. The crystalline size of nickel was ~30.3 nm, ~32.6 nm, ~33.6 nm, and ~34.6 nm, for 3NiSN after 0 h, 1.5 h, 2 h, and 2.5 h reaction on stream, respectively. The change trend of Ni size was in conformance with the catalytic activity of 3NiSN in process of CRPOM. Combined with H_2-TPR results above, with the process of CRPOM proceeding, the NiO-SiO_2 interaction over 3NiSN catalyst weakened down as it disappeared. At the same time, the crystalline size of nickel increased with the weakening of NiO-SiO_2 interaction, finally leading to the sintering of active nickel particles over 3NiSN catalyst.

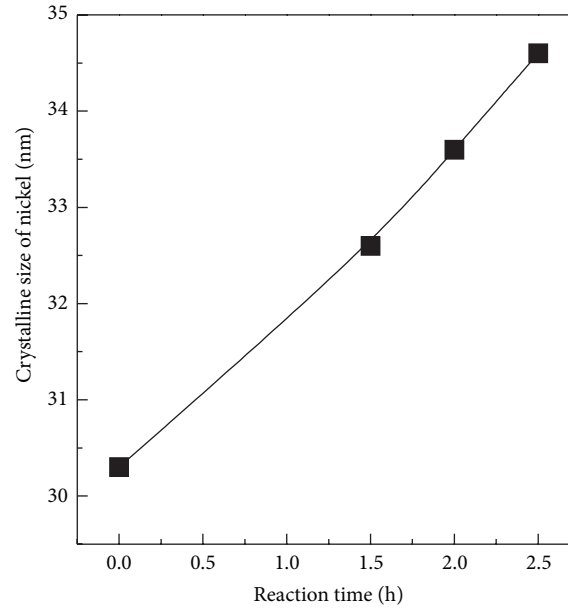

Figure 9: Crystalline size of nickel as a function of reaction time.

By comprehensively analyzing the characterization results, important information could be concluded. On one hand, graphic carbon was not detected in the spent 3NiSN catalyst by XRD and TEM, suggesting that no carbon deposition was formed during the reaction. On the other hand, except for the characteristic XRD peak of metallic nickel, no other nickel species (such as NiO) was detected, indicating that the transformation of active metallic Ni was not the reason for deactivation of 3NiSN. Importantly, the weak interaction between Ni and support disappeared as

the reaction proceeding, resulting in sintering of active nickel particles. This was the reason that 3NiSN catalyst showed a rapid deactivation in the CRPOM reaction.

4. Conclusions

In this work, Ni/SiO_2 catalysts were prepared with nickel nitrate precursor by IWI method and characterized by FT-IR, TG-DTA, UV-Raman, XRD, TEM, and H_2-TPR. By being calcined around 380°C, water and nitrate were volatilized absolutely to form NiO, which could be reduced into metallic Ni after being treated with H_2 at 700°C. The active nickel particles (around 37.5 nm) of 3NiSN catalyst were dispersed highly but weakly interacted with SiO_2 support. However, this weak interaction disappeared after repeating oxidation-reduction-oxidation in the fluidized bed reactor at 700°C. Therefore, 3NiSN catalyst suffered from obvious sintering of the active nickel particle. In light of these, a rapid deactivation of 3NiSN was shown in the process of combination of CO_2 reforming and partial oxidation of methane (CRPOM) to produce syngas.

Conflict of Interests

The authors declare that there is no conflict of interests regarding the publication of this paper.

Acknowledgments

The authors thank the financial supports of National Natural Foundation of China (nos. 21003066, 21367015, and 51068010) and Zhejiang Province Key Science and Technology Innovation Team (2012R10014-03).

References

[1] B. Pawelec, P. Castaño, J. M. Arandes et al., "Katalizatory niklowe i rutenowo-niklowe na nośnikach zawierających zeolit ZSM-5 i tlenek glinu. Wybrane właściwości fizykochemiczne i katalityczne," *Applied Catalysis A: General*, vol. 7, no. 7, pp. 20–33, 2007.

[2] T. V. Choudhary and V. R. Choudhary, "Energy-efficient syngas production through catalytic oxy-methane reforming reactions," *Angewandte Chemie*, vol. 47, no. 10, pp. 1828–1847, 2008.

[3] K.-R. Hwang, S.-W. Lee, S.-K. Ryi, D.-K. Kim, T.-H. Kim, and J.-S. Park, "Water-gas shift reaction in a plate-type Pd-membrane reactor over a nickel metal catalyst," *Fuel Processing Technology*, vol. 106, pp. 133–140, 2013.

[4] D. P. Liu, X.-Y. Quek, H. H. A. Wah, G. M. Zeng, Y. D. Li, and Y. H. Yang, "Carbon dioxide reforming of methane over nickel-grafted SBA-15 and MCM-41 catalysts," *Catalysis Today*, vol. 148, no. 3-4, pp. 243–250, 2009.

[5] V. R. Choudhary, B. S. Uphade, and A. S. Mamman, "Partial oxidation of methane to syngas with or without simultaneous CO_2 and steam reforming reactions over $Ni/AlPO_4$," *Microporous and Mesoporous Materials*, vol. 23, no. 1-2, pp. 61–66, 1998.

[6] E. Ruckenstein and Y. H. Hu, "Combination of CO_2 reforming and partial oxidation of methane over NiO/MgO solid solution catalysts," *Industrial and Engineering Chemistry Research*, vol. 37, no. 5, pp. 1744–1747, 1998.

[7] J. Newnham, K. Mantri, M. H. Amin, J. Tardio, and S. K. Bhargava, "Highly stable and active Ni-mesoporous alumina catalysts for dry reforming of methane," *International Journal of Hydrogen Energy*, vol. 37, no. 2, pp. 1454–1464, 2012.

[8] M. García-Diéguez, I. S. Pieta, M. C. Herrera, M. A. Larrubia, and L. J. Alemany, "Nanostructured Pt- and Ni-based catalysts for CO_2-reforming of methane," *Journal of Catalysis*, vol. 270, no. 1, pp. 136–145, 2010.

[9] L. Yao, J. Zhu, X. Peng, D. Tong, and C. Hu, "Comparative study on the promotion effect of Mn and Zr on the stability of Ni/SiO_2 catalyst for CO_2 reforming of methane," *International Journal of Hydrogen Energy*, vol. 38, no. 18, pp. 7268–7279, 2013.

[10] S. Tada, T. Shimizu, H. Kameyama, T. Haneda, and R. Kikuchi, "Ni/CeO_2 catalysts with high CO_2 methanation activity and high CH_4 selectivity at low temperatures," *International Journal of Hydrogen Energy*, vol. 37, no. 7, pp. 5527–5531, 2012.

[11] I. Rossetti, C. Biffi, C. L. Bianchi et al., "Ni/SiO_2 and Ni/ZrO_2 catalysts for the steam reforming of ethanol," *Applied Catalysis B: Environmental*, vol. 117-118, pp. 384–396, 2012.

[12] X. L. Yan, Y. Liu, B. R. Zhao, Y. Wang, and C.-J. Liu, "Enhanced sulfur resistance of Ni/SiO_2 catalyst for methanation *via* the plasma decomposition of nickel precursor," *Physical Chemistry Chemical Physics*, vol. 15, no. 29, pp. 12132–12138, 2013.

[13] W. S. Xia, Y. H. Hou, G. Chang, W. Z. Weng, G.-B. Han, and H.-L. Wan, "Partial oxidation of methane into syngas (H_2 + CO) over effective high-dispersed Ni/SiO_2 catalysts synthesized by a sol-gel method," *International Journal of Hydrogen Energy*, vol. 37, no. 10, pp. 8343–8353, 2012.

[14] L. Li, S. He, Y. Song, J. Zhao, W. Ji, and C.-T. Au, "Fine-tunable Ni@porous silica core-shell nanocatalysts: synthesis, characterization, and catalytic properties in partial oxidation of methane to syngas," *Journal of Catalysis*, vol. 288, pp. 54–64, 2012.

[15] D. P. Liu, Y. F. Wang, D. M. Shi et al., "Methane reforming with carbon dioxide over a Ni/ZiO_2-SiO_2 catalyst: influence of pretreatment gas atmospheres," *International Journal of Hydrogen Energy*, vol. 37, no. 13, pp. 10135–10144, 2012.

[16] M. V. Bykova, D. Y. Ermakov, V. V. Kaichev et al., "Ni-based sol-gel catalysts as promising systems for crude bio-oil upgrading: guaiacol hydrodeoxygenation study," *Applied Catalysis B: Environmental*, vol. 113-114, pp. 296–307, 2012.

[17] M. Xue, S. Hu, H. Chen, Y. Fu, and J. Shen, "Preparation of highly loaded and dispersed Ni/SiO_2 catalysts," *Catalysis Communications*, vol. 12, no. 5, pp. 332–336, 2011.

[18] R. Nares, J. Ramírez, A. Gutiérrez-Alejandre, and R. Cuevas, "Characterization and hydrogenation activity of Ni/Si(Al)—MCM-41 catalysts prepared by deposition-precipitation," *Industrial and Engineering Chemistry Research*, vol. 48, no. 3, pp. 1154–1162, 2009.

[19] A. Corma, A. Martinez, V. Martinezsoria, and J. B. Monton, "Hydrocracking of vacuum gasoil on the novel mesoporous MCM-41 aluminosilicate catalyst," *Journal of Catalysis*, vol. 153, no. 1, pp. 25–31, 1995.

[20] T. Halachev, R. Nava, and L. Dimitrov, "Catalytic activity of (P)NiMo/Ti-HMS and (P)NiW/Ti-HMS catalysts in the hydrogenation of naphthalene," *Applied Catalysis A: General*, vol. 169, no. 1, pp. 111–117, 1998.

[21] S. He, H. Wu, W. Yu, L. Mo, H. Lou, and X. Zheng, "Combination of CO_2 reforming and partial oxidation of methane to produce syngas over Ni/SiO_2 and $Ni–Al_2O_3/SiO_2$ catalysts with different precursors," *International Journal of Hydrogen Energy*, vol. 34, no. 2, pp. 839–843, 2009.

[22] S. F. He, Q. S. Jing, W. J. Yu, L. Y. Mo, H. Lou, and X. M. Zheng, "Combination of CO_2 reforming and partial oxidation of methane to produce syngas over Ni/SiO_2 prepared with nickel citrate precursor," *Catalysis Today*, vol. 148, no. 1-2, pp. 130–133, 2010.

[23] S. He, X. Zheng, L. Mo, W. Yu, H. Wang, and Y. Luo, "Characterization and catalytic properties of Ni/SiO_2 catalysts prepared with nickel citrate as precursor," *Materials Research Bulletin*, vol. 49, pp. 108–113, 2014.

[24] E. Marceau, M. Che, J. Čejka, and A. Zukal, "Nickel(II) nitrate vs. acetate: influence of the precursor on the structure and reducibility of Ni/MCM-41 and Ni/Al-MCM-41 catalysts," *ChemCatChem*, vol. 2, no. 4, pp. 413–422, 2010.

[25] J. Chen and Q. Z. Song, *Organic Spectral Analysis*, BIT Press, Beijing, China, 1996.

[26] J. F. Xu, W. Ji, Z. X. Shen et al., "Raman spectra of CuO nanocrystals," *Journal of Raman Spectroscopy*, vol. 30, no. 5, pp. 413–415, 1999.

[27] H. Richter, Z. P. Wang, and L. Ley, "The one phonon Raman spectrum in microcrystalline silicon," *Solid State Communications*, vol. 39, no. 5, pp. 625–629, 1981.

[28] Z. Zhao, Y. Yamada, A. Ueda, H. Sakurai, and T. Kobayashi, "The roles of redox and acid-base properties of silica-supported vanadia catalysts in the selective oxidation of ethane," *Catalysis Today*, vol. 93–95, pp. 163–171, 2004.